X-ray micro CT for studying strain localization in clay rocks under triaxial compression

Pierre Bésuelle, Gioacchino Cinno Viggiani, Nicolas Lenoir, Jacques Desrues, Michel Bornert

X-ray Micro CT for Studying Strain Localization in Clay Rocks under Triaxial Compression

Bésuelle P.* — Viggiani G.* — Lenoir N. — Desrues J.* — Bornert M.*****

** Laboratoire 3S, BP 53, 38041 Grenoble cedex 9, France*
Pierre.Besuelle@hmg.inpg.fr, Cino.Viggiani@hmg.inpg.fr, Jacques.Desrues@hmg.inpg.fr

*** formerly at ANDRA and Laboratoire 3S*
now at University of Kumamoto, Japan
Nicolas.Lenoir@hmg.inpg.fr

**** Laboratoire de Mécanique des Solides, 91128 Palaiseau cedex, France*
bornert@lms.polytechnique.fr

ABSTRACT: *The paper presents selected results from an experimental testing program recently performed at the ESRF, where high resolution, fast X-ray micro tomography was used to evaluate the onset and evolution of strain localization in Callovo-Oxfordian argillite under deviatoric loading. In situ micro tomography allowed detailed observations of strain localization at different load levels. X-ray CT was complimented with 3D digital image correlation to obtain a sequence of incremental 3D strain fields of a deforming specimen.*

KEY WORDS: *in situ micro tomography, synchrotron, triaxial compression, strain localization, cracks, 3D digital image correlation*

---

1. Introduction

Strain localization, the concentration of deformation into narrow zones of intense shearing, is a phenomenon commonly observed in virtually all geomaterials, including rocks, soils and concrete. Experimental investigations represent an essential ingredient for improving the understanding of the mechanics and physics of shear banding. A wide range of experimental techniques have been applied over the years, which include optical and electronic microscopy, radiographic analysis, ultrasonic and acoustic techniques, multiple stress and strain local measurements, stereophotogrammetry and digital image analysis to name but a few. The challenge here, and the possible reason why so many different techniques have been used is the fact that one wants to measure deformations in a region the size of which, upon strain localization, reduces abruptly and dramatically, say from the scale of the specimen to the shear band scale. Measuring deformations throughout a test, that is: prior to, at, and after the onset of strain localization is then a formidable task, which can only be accomplished by using *field measurements*. In fact, it should be stressed that when strains are (highly) localized, stress and strain variables cannot be derived from boundary measurements of loads and displacements.

In principle, direct three dimensional (3D) observation of the internal structure of a specimen while it deforms under applied load can provide substantial advances in the understanding of shear banding in geomaterials. In this respect, the recent, rapid development of non destructive 3D imaging techniques such as X-ray tomography (*e.g.*, Baruchel *et al*., 2000) offers new experimental possibilities, which have been indeed used in recent years for studying shear banding and failure in geomaterials. However, several requirements specific to geomaterials – confining pressure and pore pressure control – make it quite difficult to properly run a test within a typical X-ray tomography set up, especially if one intends to perform *in situ* tomography, *i.e.*, to load the specimen and to scan it in the same setting and at the same time (*e.g.*, Otani *et al*., 2002; Raynaud *et al.*, 1989; Desrues *et al.*, 1996; Otani *et al.*, 2000; Alshibli *et al.*, 2000; Vinegard *et al.* 1991; Kawakata *et al.*, 1999).

It should be noted that all the above experimental studies have been performed with conventional Computed Tomography (CT) systems used in medical and industrial applications. However, another, much more powerful source of X-rays can be provided by the synchrotron radiation, for which the X-ray beam is a thousand billion times “brighter” than the beam produced by a hospital X-ray machine. The higher energy and photon flux of synchrotron radiation allow for a much higher resolution, down to the micrometric scale.

Such a resolution is probably unnecessary for coarse-grained geomaterials such as sand, in which the width of a shear band is known to be roughly 10 to 20 times the mean grain diameter size (*i.e.*, within a few millimeters). However, it becomes crucial for characterizing strain localization in fine-grained materials such as clays, marls and clayey rocks, in which shear bands are much thinner, and are often described as displacement discontinuities, or slip surfaces (Viggiani *et al.*, 2004). This is apparent from the relatively poor quality of the (few) available tomographic images of shear zones in fine-grained geomaterials obtained so far (Otani *et al*., 2000; Tillard-Ngan, 1992; Hicher *et al*., 1994).

Another difficulty with experimentally detecting strain localization is associated to the very nature of localized strain. In fact, while localization can sometimes induce large volumetric deformation – either dilatancy (or crack opening) or compaction (compaction bands), depending on the material and loading conditions – in general *volumetric* strain in a shear band is small compared to the *shear* strain. Unfortunately, X-ray CT is based on transmission measurement, hence it is sensible to density variations only. Therefore, in the absence of measurable volumetric strain in the region of localized deformation, X-ray CT may fail to detect the phenomenon, especially in its early stage (Bésuelle, 2003). As it will be shown in the paper, such a limitation can be overcome by complimenting X-ray CT with digital image correlation (DIC). Through the comparison of couples of reconstructed 3D images of a specimen at two successive steps of loading, this allows to measure an incremental displacement field, from which a strain tensor field can be obtained.

This paper presents a few selected results from a recent, unique experimental testing program where synchrotron radiation micro tomography has been used to evaluate the onset and evolution of localized deformation in a fine-grained clayey rock under deviatoric loading. A brief description of the material tested is first given in Section 2. Section 3 describes the apparatus which was specifically designed to be placed in the X-ray beam (*in-situ* tomography) at the ESRF. A few results from X-ray CT are discussed in Section 4. Then, DIC is presented in Section 5 together with a few representative results. Finally, some conclusions are drawn in Section 6.

2. Material Tested

The argillite tested for this study was provided by ANDRA (*Agence Nationale pour la Gestion des Déchets Radioactifs*) from their underground research laboratory (URL) site at Bure (Meuse/Haute Marne, Eastern France).

It belongs to the Callovo-Oxfordian Formation (Jurassic), which is about 130 m thick in the area of the URL, with its base at about 550 m below the ground surface. Core samples of 100 mm diameter and 320 mm length were taken at different depths between 476 and 479 m below the surface from the drill core of the boreholes EST212 and EST361 drilled at the axis of the auxiliary shaft of the URL. A candidate for the geological disposal of radioactive waste, the Callovo-Oxfordian argillite has been in recent years the object of many detailed studies (*e.g.*, Escoffier 2002, Zhang *et al.* 2004, Escoffier *et al.* 2005, Fabre and Pellet 2006). At the investigated depth, the material has an extremely low intrinsic permeability (10^{-20} to 10^{-22} m^2) and a uniaxial compressive strength ranging from 20 to 30 MPa. Its water content is equal to about 6%, and clay content is in range 40 to 45%, the other minerals being essentially calcite and quartz. In order to prevent loss of water and possible damages, the samples after drilling were stored in sealing cells. Cylindrical specimens (10 mm in diameter and 20 mm in height) were prepared by cutting from the cores by means of a diamond wire saw, which minimizes material disturbance during preparation (see Lenoir 2006 for details).

3. Experimental Set-up

3.1. *Micro tomography Device*

The experiments were carried out at the high energy beamline ID15A at the European Synchrotron Radiation Facility (ESRF) in Grenoble, a third generation storage ring. This beamline has been recently equipped with a fast three-dimensional X-ray micro tomography system (Di Michiel *et al.*, 2005). In fact, the work presented in this paper is one of the first applications of fast micro tomography at ID15A. The setup is schematically shown in Figure 1a. The X-ray white radiation was generated by an 11 poles wiggler, in order to get a high photon flux. The X-ray energy used for this study ranged from 50 to 70 keV, and the radiation was filtered using a stack of polymer pieces, in order to avoid beam hardening artifacts. The triaxial apparatus (including the loading system, confining cell and specimen) was moved and rotated by a high precision positioning device in order to get a sequence of digital radiographs at different angular positions and different elevations. The X-rays transmitted through the two polycarbonate cell walls, the confining fluid, and the claystone specimen, were converted into visible light by a phosphor screen scintillator. A 1024×1024 *Dalstar* CCD camera captured the raw digital images from the phosphor screen. The pixel size was 14×14 μm^2, and a 1X objective was used for the scans described hereafter. The size of the beam was 14×3.65 mm^2, which allows to get, for each radiograph, 261 slices of the specimen (10 mm in diameter). The exposure time was equal to 0.04 s for each

radiograph, and the complete scan of a section, obtained by taking 1200 radiographs at different equally spaced angles covering a range of 180°, took approximately 2.5 minutes. The acquisition of the entire specimen height (20 mm) took no more than 15 minutes, with a voxel size of 14×14×14 μm^3.

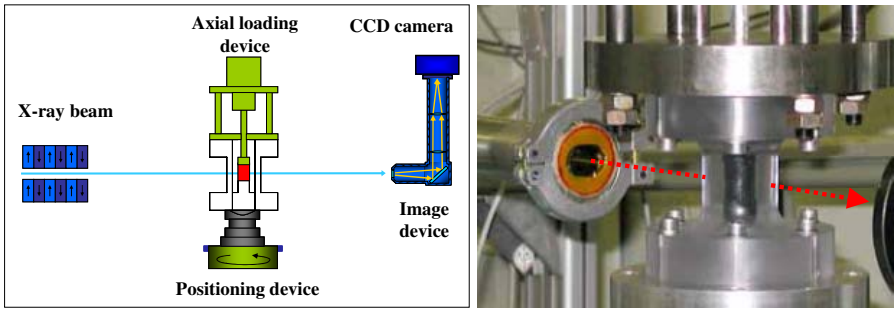

(a) (b)

Figure 1. *(a) scheme of the micro-CT device; (b) experimental setup showing a specimen inside the transparent triaxial cell*

3.2. *Triaxial Apparatus and Testing Program*

The apparatus includes a small triaxial cell and a loading device designed specifically for this program (Viggiani *et al.*, 2004). The triaxial apparatus is practically the same as a conventional triaxial testing system, except for its much smaller size and the shape of the confining cell, which was designed to be as transparent as possible to the X-rays. The rock specimen is a cylinder with height twice the diameter (20 and 10 mm, respectively). The top and bottom rigid platens are enlarged and lubricated to minimize friction at the ends of the specimen. The specimen is enclosed in a thin neoprene sleeve sealed to the top and bottom platens, and placed in an oil-filled cell, which can sustain up to 10 MPa. A frictionless ram passes through the top of the cell and allows applying a stress deviator $q = (\sigma_a - \sigma_r)$, σ_a and σ_r being the axial and radial total stress, respectively. The axial strain, ε_a, is obtained by measuring the movement of the ram using a LVDT.

The axial load and hence the deviator stress is applied in a displacement-controlled manner using a motor-driven screw actuator. The loading system was designed in cooperation with CSP (*Composants et Systèmes de Précision*) and can be placed in the X-ray beamline without interfering with the tomographic scans. It is quite compact and light (less than 30 kg), which is

important since it directly sits on the translation and rotation stage during the experiment. The system has a maximum loading capacity of 7.5 kN, and allows to move the ram at a constant rate in the range of 1 to 100 µm/min. It is worth noting that while in a conventional triaxial system the tensile reaction force is carried by a loading frame, in this case it is carried by the cell walls, which therefore are subjected to traction in the axial direction. This allows a clear path, free of any obstacle (apart from the cell walls), for the X-ray beam within the region to be scanned. X-ray absorption through the apparatus must be small, so the walls of the cell have to be as thin as possible. In the mean time, they cannot be too thin, as they must resist the axial traction — in addition to the cell pressure. The solution adopted was to reduce the thickness of the polycarbonate walls to a value of 10 mm only where needed, *i.e.* in the central region of the cell. The output signals of all transducers (for axial load, cell pressure, and axial strain) are conditioned by a 16 bit process interface unit which is linked to a laptop computer, which also controls the loading actuator. The experiments are remotely controlled from a control cabin, because the shield room, the so-called *experimental hutch*, is obviously inaccessible when the shutter is open.

A total of four triaxial compression tests on Callovo-Oxfordian argillite were performed, at three different values of the confining stress (1, 5 and 10 MPa). The tests were carried out under undrained conditions, *i.e.*, no drainage of the pore fluid into, or out of, the specimen was allowed. See Lenoir (2006) for further details.

4. Selected Results

Results from only two tests (*ESTSYN01* and *ESTSYN02*) are presented herein. The confining pressure (total mean stress) was equal to 10 MPa and 1 MPa, respectively. Deviatoric loading was performed under displacement control, by advancing the loading ram at a rate of 3.0 µm/min, which corresponds to a nominal axial strain rate of $2.5.10^{-6}$ s^{-1} for a 20 mm specimen height. For each test, the specimen was scanned at different steps: before and right after applying the confining pressure (steps 0 and 1, respectively), and then at different levels of axial strain during deviatoric loading (steps 2-7 for test *ESTSYN01* and steps 2-5 for test *ESTSYN02*). One last scan of the specimen was performed at the end of the test, after removal of the confining pressure (step 8 for test *ESTSYN01* and step 6 for test *ESTSYN02*). It is worth to note that the ram displacement was stopped at those points of the test when a tomographic scan of the specimen was required. The specimen was scanned while the axial strain was held constant, which unavoidably caused some amount of axial load relaxation during scanning. However, the scanning

operations were fast enough (approximately 15 minutes for six sections, *i.e.*, the full specimen height) for this relaxation to be relatively small.

Deviator stress q is plotted as a function of axial strain ε_a in Figure 2 for both tests. All stresses and strains are positive in compression. The numbers noted on each curve are the scanning step numbers. In test *ESTSYN01*, the deviator stress first increases (almost linearly up to step 2), then attains a peak value of 28 MPa around step 3 and finally decreases, essentially leveling off at about 19 MPa after step 5. A single shear band formed in the specimen during the test, which could be clearly observed by the eye at the end of the test.

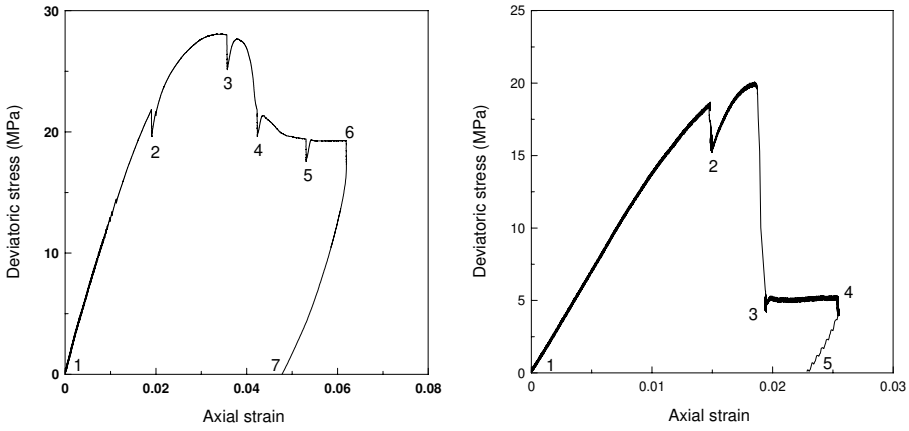

Figure 2. *Deviator stress vs. axial strain for test ESTSYN01 (10MPa confining stress, left) and test ESTSYN02 (1MPa confining stress, right)*

We focus now on the X-ray CT scans of specimen *ESTSYN01* during loading. Figure 3 shows the reconstruction of a tomographic slice perpendicular to the specimen's axis for each scanning step. Note that the elevation of a given slice decreases from one scan to the next, to take into account the specimen shortening during loading. Strain localization becomes visible at step 4 as a very narrow band in the upper left part of the slice. The band of localized deformation appears as a darker zone (2-3 pixels, *i.e.*, 30-40 µm thick), which means that the material is dilating inside the band (darker indicates lower mass density). In the subsequent scanning steps, the band becomes increasingly visible in term of both length and thickness (about 60 µm at step 7), essentially in the outer region of the slice. A material shift can be observed at the intersection of the band with the external surface of the

specimen. The size of such shift increases with specimen shortening, which is due to the relative sliding on the band. When the confining pressure is removed (step 8), the band of localization opens up in the outer region of the specimen and it looks like an open crack. However, no trace of localization is visible in the central region of the slice.

By performing a 3D reconstruction, it is possible to obtain a virtual slice in a plane orthogonal to the slices in Figure 3, *i.e.*, parallel to the specimen's axis. In such a plane, the region of localization appears as a straight band. Interestingly, the existence of distinct inclusions of calcite in the argillite turned out to be particularly helpful for characterizing shear sliding along the band. In fact, some of these inclusions, which are due to the activity of bio-organisms during sedimentation of the clay particles, have a quite elongated vein shape and a length of a few millimeters (Figure 4a), thus appearing as distinct thin white bands in a CT image. A specific analysis based on a gray level separation, allowed to recognize these inclusions as well as the open fissures (respectively shown in yellow and in red in Figure 4b). It appears that upon loading, the vein-shaped inclusion shown in Figure 4 was strongly deformed by the band of localization (compare Figure 4a at step 1 and Figure 4b at step 8).

The evolution of the inclusion geometry throughout test *ESTSYN01* is shown in Figure 4c. Some shearing of the inclusion is apparent starting from step 5, and becomes more and more pronounced for increasing deformation (steps 6 through 8). However, the region of intense shearing in the shale is not associated to a measurable variation of density (at least within the X-ray CT resolution, which is based on X-ray absorption). This implies that the band of localization in the central zone of the specimen is essentially a shear band without substantial volumetric deformation, whereas some localized volume changes (eventually, crack opening) can be observed as the region of localized deformation is closer to the edge of the slice.

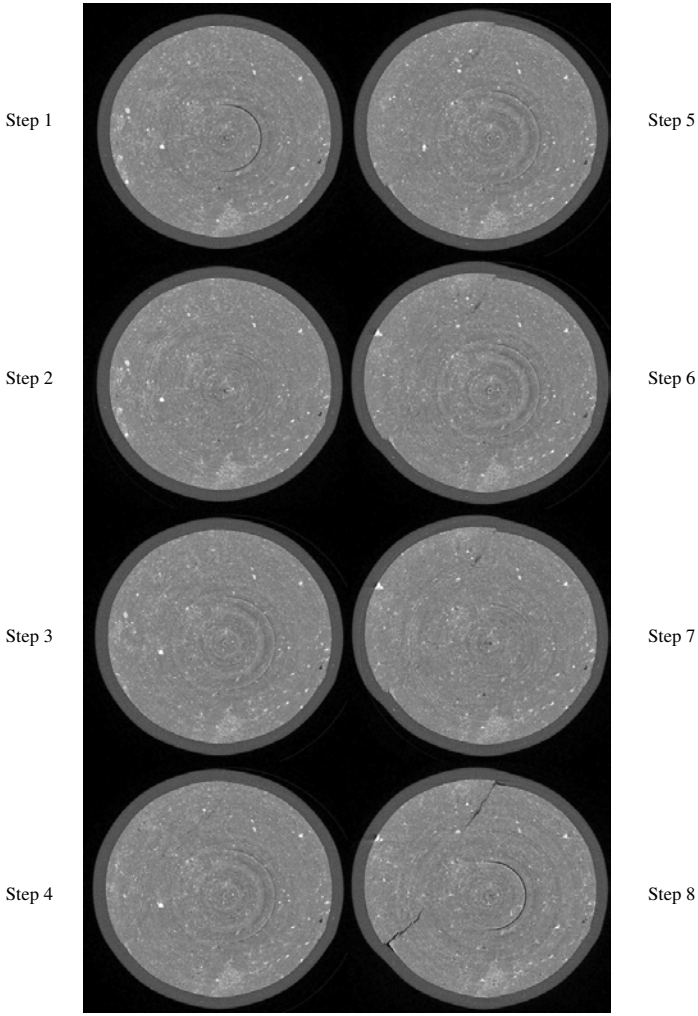

Figure 3. *A horizontal CT slice of specimen ESTSYN01 at different steps*

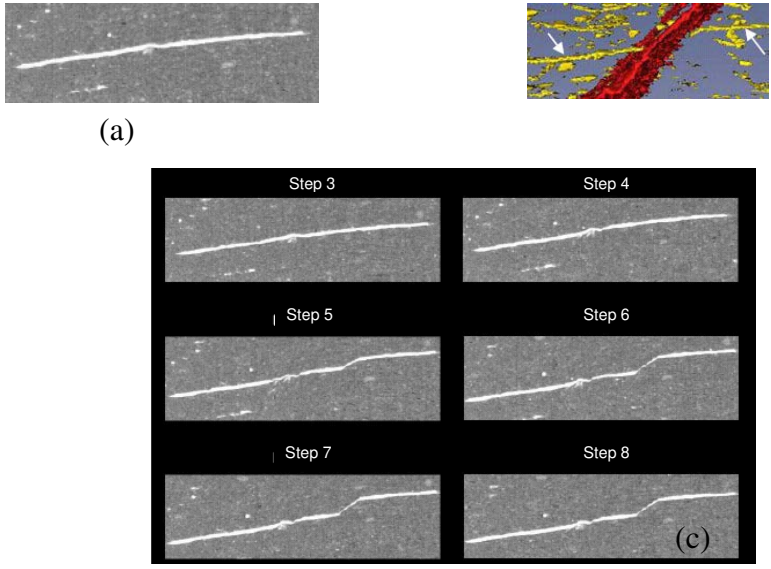

Figure 4. *A natural vein-shaped inclusion in specimen ESTSYN01: (a) CT image in a vertical plane before loading (step 1), (b) 3D reconstruction after unloading (step 8), and (c) CT image in a vertical plane at different steps of loading*

Test *ESTSYN02* exhibited a much more brittle behavior, see Figure 2. The deviator stress drops from 20 MPa down to about 5 MPa immediately after the peak, and stays constant in the post-peak portion of the test. At the end of the test, the specimen was split into several pieces. Figure 5 shows the evolution of three tomographic slices at different elevations (11.0, 7.2 and 3.6 mm from the bottom of the specimen, respectively) throughout the test. At the lower elevation, localized deformation is visible already at step 2, appearing as two dark (*i.e.*, dilating) zones a few pixels wide. These bands include a few segments which can be also interpreted as open cracks. The regions of localization are in any case extremely thin with respect to the spatial resolution, which sometime makes it difficult to discriminate between a dilating band and an opening crack. At step 3, several fissures can be observed on all three slices. Their opening increases thereafter, especially after the removal of confining pressure (step 6), when a well developed network of fissures has developed at the lower elevation. A 3D reconstruction of the data for test *ESTSYN02* (not shown herein) allowed to recognize that while some of these fissures are vertical (axial splitting), also inclined fissures developed in the specimen, so that the overall spatial organization of the fissures is quite complex (see Lenoir 2006 for details).

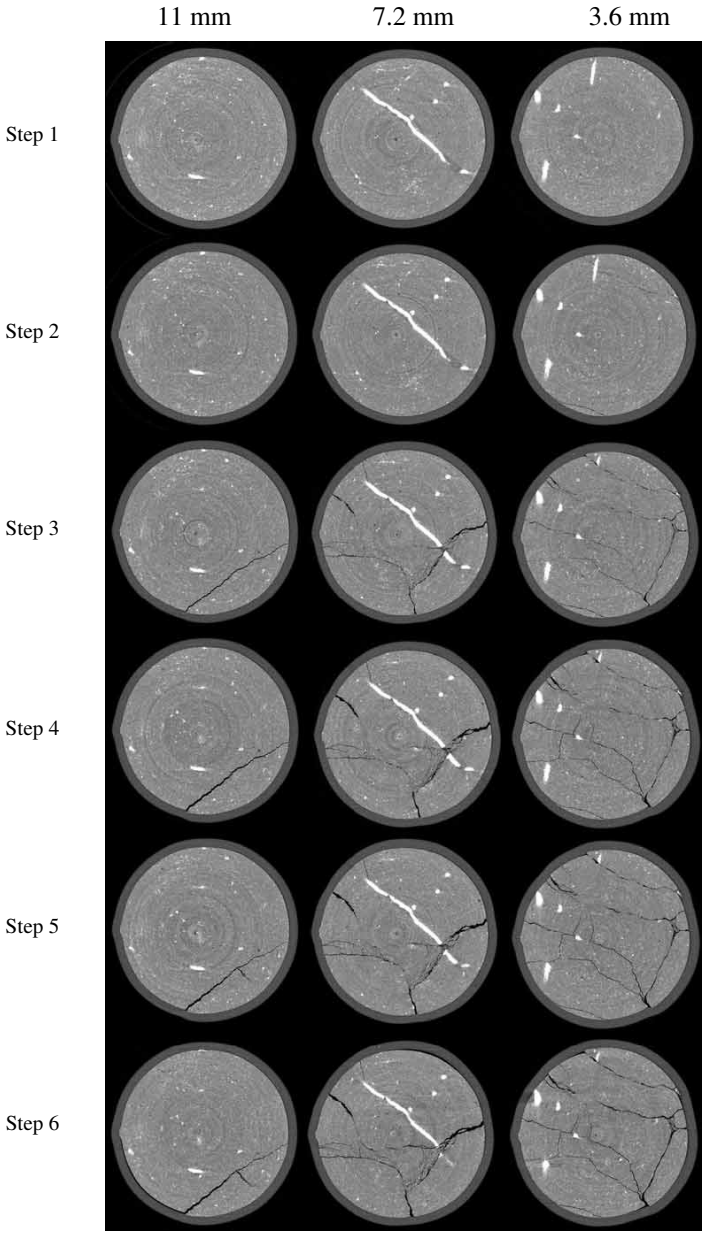

Figure 5. *Horizontal CT slices of specimen ESTSYN02 at different steps and for three different elevations*

5. Strain Field Measurement by Digital Image Correlation

Direct observation of X-ray micro tomography images allows for immediately detecting volumetric strain, since dilation (contraction) corresponds to a change of mass density, which in turn results in a decrease (increase) of X-ray attenuation. However, as far as shear (deviatoric) strain is concerned, this does not necessarily induce any volume change and therefore it cannot be directly detected by measuring changes in X-ray attenuation. In this study, we have developed a general method for obtaining the distribution of both the volumetric and deviatoric components of strain increment between two reconstructions of a specimen at two different steps of deformation. The method, which is based on the correlation of digital volume (3D) tomographic images, is thoroughly described elsewhere (Lenoir *et al.*, 2006). Herein, only a short explanation of the method will be given, along with some background on 3D DIC. Then, a few representative results will be shown of 3D strain fields obtained for test *ESTSYN01*.

Digital Image Correlation (DIC, hereafter) is a mathematical method which essentially consist in recognizing the same material point on a pair of digital images of an object. A material point is assumed to be fully identified by its local pattern (*e.g.*, the gray level distribution around the point in a black and white image). Such a local pattern is assumed to be unique for a given point, *i.e.*, it cannot be found elsewhere on the image. By optimizing an appropriate correlation function, DIC allows for determining for each point/pattern on the first image, the most likely location of such a point/pattern on the second image. Note that from one image to the other, a pattern is in general subject to translation, rotation and distortion. By repeating this procedure for a number of points, a full displacement and deformation field can be obtained for the pair of images.

Such a method was applied to measure 2D displacement and deformation fields on the surface of a specimen already back in the 80s (Chu *et al.*, 1985; Bruck *et al.*, 1989). Since, DIC techniques have become widely used in geomechanics (*e.g.*, Gudehus and Nübel, 2004; Bhandari and Inoue, 2005 – to mention just a few recent studies). Note that using two rather than just one digital camera, one can measure 3D displacements on the surface of a specimen (*e.g.*, Helm *et al.*, 1996). However, surface displacement fields are not necessarily representative of the deformation inside a specimen, except in some particular cases (*e.g.*, specimens loaded in plane strain).

DIC has also been applied to X-ray photographs (Russel and Sutton, 1989; Synnergen *et al.*, 1999). In this case, the pattern is the X-ray attenuation distribution through the specimen in the direction of propagation of the rays. More recently, full three dimensional displacement and strain fields have been measured based on X-ray (micro-) CT reconstructions (Bay *et al*., 1999, Smith *et al.*, 2002; Verhulp *et al*., 2004; Bornert *et al*. 2004b; Forsberg and Sjödahl, 2004). The particular 3D DIC method

used in the present study is similar to that described by Bornert *et al.* (2004a). Additional information on its application to the present CT images of clayey rocks are given elsewhere (Lenoir *et al.*, 2006). Herein it will be sufficient to bear in mind that each 3D image is decomposed in several subsets, which are cubes in the reference image, each of them containing 20^3 voxels. The center of a subset is identified by the gray level distribution inside the subset. Also note that due to the small deformation experienced by the argillite specimens, for this study the transformation between two images was assumed to be a rigid translation, without any rotation and distortion. While such an approximation substantially reduced the computing time, it still provided a fair resolution (see Lenoir *et al.*, 2006 for further details).

Hereafter, a few results are presented where DIC was applied to the 3D tomographic images from test *ESTSYN01*. Only the two increments between steps 2 and 3 and between steps 3 and 4 are discussed herein (see Figures 2 and 3). Hereafter, these two increments will be referred to as the pre-peak and the post-peak increment, respectively. Figures 6 and 7 show the (incremental) strain field as obtained by DIC. More precisely, these fields represent the second invariant of the strain tensor, in the sense of von Mises, which is a measure of shear strain. To better appreciate the computed 3D fields, these are also shown by a few horizontal and vertical cuts (see respectively left and right images on Figures 6 and 7). The maximum strain plotted in these figures equals 0.15, which means that the red color indicates shear strain values equal to, or greater than 0.15.

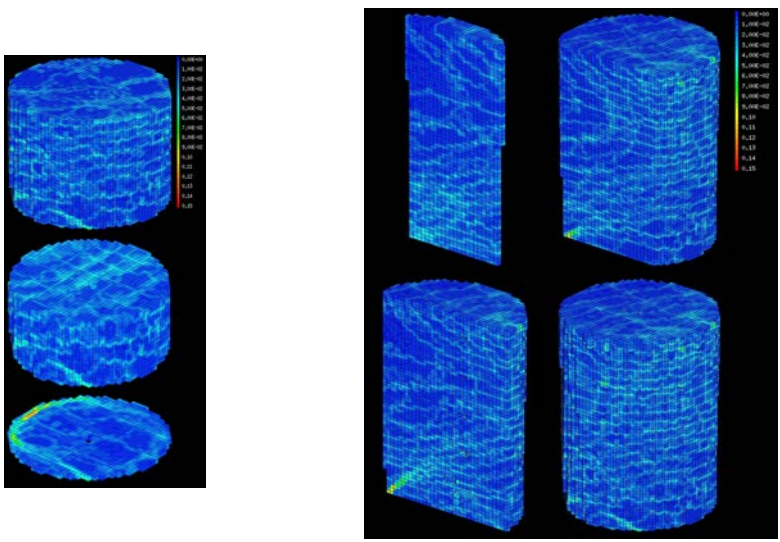

Figure 6. *Three dimensional shear strain increment field in the pre-peak increment, represented by horizontal cuts at different heights (left), and vertical cuts (right)*

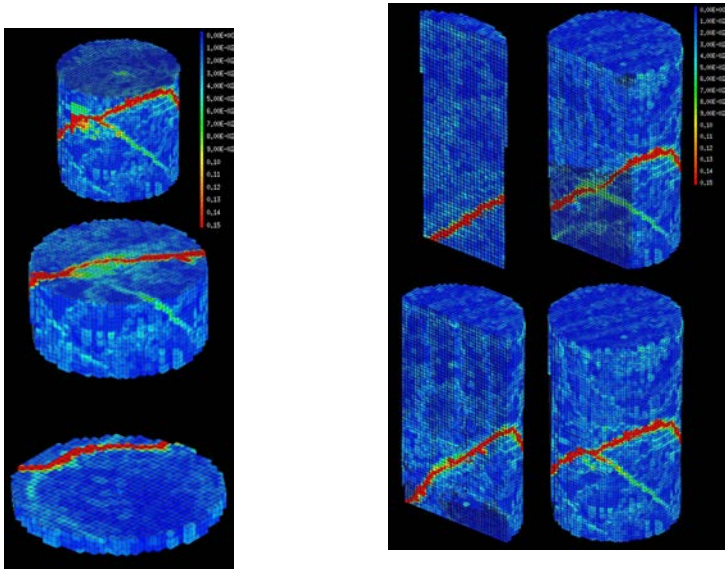

Figure 7. *Three dimensional shear strain increment field in the post-peak increment, represented by horizontal cuts at different heights (left), and vertical cuts (right)*

Strain localization is distinctly visible already in the pre-peak increment (Figure 6), close to the bottom edge of the specimen. Such a shear zone appears as a narrow, straight band in the vertical cuts. The shape of the shear zone is circular in the horizontal bottom cut, which suggests that the overall shape of the zone of localized deformation is influenced to some extent by the boundary conditions. In the post-peak increment (Figure 7), the shear band has entirely propagated through the specimen. As compared to the pre-peak increment, the zone of localized deformation appears straight (planar) both in the vertical and in the horizontal cuts. A second shear band can also be observed, which is characterized by lower values of the (incremental) shear strain. A closer scrutiny of the 3D tomographic images revealed that very close to the intersection of these two bands, in the external part of the specimen, a large inclusion of calcite and pyrite existed in the argillite. This inclusion is in fact also revealed by the green volume (a few subsets in size) which appeared on the 3D strain fields in Figure 7 (see top left and bottom right images). Such an inclusion was most likely stiffer than the matrix, which induced a shear strain concentration. Therefore, it can be concluded that in test *ESTSYN01*, the pattern of localization was influenced by both the boundary conditions (at the specimen bottom) and natural inclusions in the specimen. Fields of the first invariant of the strain tensor (*i.e.*, the volumetric strain) were also computed for test *ESTSYN01*, which are not reported herein (see Lenoir, 2006). These fields indicate

that volume changes localized only in the post-peak increment. Just like the simple observation of CT images (without any DIC analysis), the inspection of volumetric strain fields allows to detect shear banding only at a later stage of the test, when dilatancy and/or crack opening induced measurable mass density variations.

Finally, it is worth to note that the thickness of the shear bands as it appears in these DIC-based shear strain fields is largely over evaluated, because it cannot be smaller than the subset size. Recall that the side of the subset was equal to 20 voxels (*i.e.*, 280 µm) in this analysis, whereas CT images indicate that the thickness of the zones of localized deformation in the tested specimens was typically less than 70 µm (see Lenoir, 2006).

6. Conclusions

An original loading system has been developed for testing argillaceous rocks at a relatively high confining pressure (10 MPa), which allows for micro tomography observation of the specimen under deviatoric loading. The high energy synchrotron radiation used for this study allowed to combine both *fast* tomography and *high resolution* micro tomography. This is essential for argillites, due to the fine micro structure (with zones of localized deformation which can be only a few microns wide) and their susceptibility to creep, which makes it difficult to have a stable specimen configuration if the radiation period is too long.

X-ray tomography essentially measures material density distribution. During a test, changes of X-ray attenuation are therefore due to volumetric deformation. If the material in a zone of localized deformation is essentially strained in shear, without significant volumetric strain, then the phenomenon can be hard to detect. However, it has been shown in this study that X-ray 3D imaging can be effectively complimented with 3D digital image correlation, which allows for measuring a 3D displacement field in a specimen. From the displacement field, a 3D strain field can then be obtained, including the shear and volumetric strain components. The quality of the results that can be obtained by digital image correlation crucially depend on the quality of the images (which need to be well contrasted) as well as on the signal-to-noise ratio, that must be sufficiently high. In this study, while the use of synchrotron light allowed to meet the latter requirement, the contrast in the images directly results from the natural heterogeneity of the tested material.

Different regimes of behavior were obtained for the Callovo-Oxfordian argillite in the investigated confining stress range, from brittle (at 1 MPa) to ductile (at 10 MPa). This paper has mainly focused on the ductile behavior at higher confining stress, where a single band of localized deformation was observed and there was little to very little volumetric strain in such a band. At lower confining stresses, failure was

associated to the appearance of several open cracks, both parallel to the direction of loading (axial splitting) and inclined. In this case, the application of digital image correlation is more difficult because the specimen splits into several pieces.

7. Acknowledgements

The authors are very grateful to Marco Di Michiel from the ESRF at Grenoble for his invaluable contribution to the experimental program. We also wish to thank ANDRA for financially supporting this project and for supplying core samples from their site at *Bure*.

8. References

Alshibli K.A., Sture S., Costes N.C., Franck M.L., Lankton M.R., Batiste S.N., Swanson R.A., "Assessment of localized deformation in sand using X-ray computed tomography", *Geotechnical Testing Journal*, vol. 23, p. 274-299, 2000.

Baruchel J., Buffière J.Y., Maire E., Merle P., Peix G, *X-ray Tomography in Materials Science*, Paris, Editions Hermes, 2000.

Bay B.K., Smith T.S., Fyhrie D.P., Saad M., "Digital volume correlation: three-dimensional strain mapping using X-ray tomography", *Experimental Mechanics*, vol. 39 no. 3, p. 217-226, 1999.

Bésuelle P., "X-ray CT observations of strain localization and failure in two porous sandstones", *Proc. 1st Int. Workshop X-ray CT for Geomaterials, GeoX 2003*, Kumamoto, Japan, p. 287-292, 6-7 november 2003.

Bhandari A.R., Inoue J., "Strain localization in soft rocks – a typical rate-dependent solid: experimental and numerical studies", *International Journal for Numerical and Analytical Methods in Geomechanics*, vol. 29, p. 1087-1107, 2005.

Bornert M., Chaix J.M., Doumalin P., Dupré J.C., Fournel T., Jeulin D., Maire E., Moreaud M. and Moulinec H., "Mesure tridimensionnelle de champs cinématiques par imagerie volumique pour l'analyse des matériaux et des structures", *Instrumentation, Mesure, Métrologie*, vol. 4, p. 43-88, 2004.

Bornert M., Doumalin P., Maire E., Moulinec H., "Full 3D investigation of the local straint field in particulate metal matrix composites", *Proc. 12th Int. Conf. on Experimental Mechanics ICEM12*, Bari, Italy, p. 1-8, 29 August-2 Sept. 2004.

Bruck H.A., McNeill S.R., Sutton M.A., Peters W.H., "Digital image correlation using Newton-Raphson method of partial differential correction", *Experimental Mechanics*, vol. 29 no. 3, p. 261-267, 1989.

Chu T.C., Ranson W.F., Sutton M.A., Peters W.H., "Applications of digital-image-correlation techniques to experimental mechanics", *Experimental Mechanics*, vol. 25 no. 3, p. 232-244, 1985.

Desrues J., Chambon R., Mokni M., Mazerolle F., "Void ratio evolution inside shear bands in triaxial sand specimens studied by computed tomography", *Géotechnique*, vol. 46, p. 529-546, 1996.

Di Michiel M., Merino J.M., Fernandez-Carreiras D., Buslaps T., Honkimäki V., Falus P., Martins T., Svensson O., "Fast microtomography using high energy synchrotron radiation", *Review of Scientific Instruments*, vol. 76, 2005.

Escoffier S., Caractérisation expérimentale du comportement hydromécanique des argilites Meuse/Haute Marne, PhD thesis, Institut National Polytechnique de Lorraine, 2002.

Escoffier S., Homand F., Giraud A ., Hoteit N., Su K., "Under stress permeability determination of the Meuse/Haute-Marne mudstone", *Engineering Geology*, vol. 81, no. 3, p. 329-340, 2005.

Fabre G., Pellet F., "Creep and time-dependent damage in argillaceous rocks", *International Journal of Rock Mechanics and Mining Sciences*, vol. 43, no. 6, p. 950-960, 2006.

Forsberg F., Sjödahl M., "Tomographic 3D-DSP: measurement of internal deformations", *Proc. 12th Int. Conf. on Experimental Mechanics ICEM12*, Bari, Italy, p. 217-226, 29 august-2 sept. 2004.

Gudehus G. and Nübel K., "Evolution of shear bands in sand", *Géotechnique*, vol. 54, p. 187-201, 2004.

Helm J.D., McNeill S.R., Sutton M.A., "Improved three-dimensional image correlation for surface displacement measurement", *Optical Engineering*, vol. 35 no. 7, p. 1911-1920, 1996.

Hicher P.Y., Wahyudi H., Tessier D., "Microstructural analysis of strain localisation in clay", *Computers and Geotechnics*, vol. 16, p. 205-222, 1994.

Kawakata H., Cho A., Kiyama T., Yanagidani T., Kusunose K., Shimada H., "Three-dimensional observations of faulting process in Westerly granite under uniaxial and triaxial conditions by X-ray CT scan", *Tectonophysics*, vol. 313, p. 293-305, 1999.

Lenoir N., Comportement mécanique et rupture dans les roches argileuses étudiés par micro tomographie à rayons X, PhD thesis, Grenoble University (http://tel.ccsd.cnrs.fr/tel-00011996), 2006.

Lenoir N., Bornert M., Desrues J., Bésuelle P., Viggiani G., "3D digital image correlation applied to X-ray micro tomography images from triaxial compression tests on argillaceous rock", *Strain* (submitted), 2006.

Otani J., Mukunoki T., Obara Y., “Characterization of failure in sand under triaxial compression using an industrial X-ray scanner”, *International Journal of Physical Modelling in Geotechnics*, vol. 1, p. 15-22, 2002.

Otani J., Mukunoki T., Obara Y., “Application of X-ray CT method for characterization of failure in soils”, *Soils and Foundations*, vol. 40, p. 111-118, 2000.

Raynaud S., Fabre D., Mazerolle F., Géraud Y., Latière H.J., “Analysis of the internal structure of rocks and characterization of mechanical deformation by a non-destructive method: X-ray tomodensitometry”, *Tectonophysics*, vol. 159, p.149-159, 1989.

Russel S.S., Sutton M.A., “Strain-field analysis acquired through correlation of X-ray radiographs of a fiber-reinforced composite laminate”, *Experimental Mechanics*, vol. 29 no. 2, p. 237-240, 1989.

Smith T.S., Bay B.K., Rashid M.M., “Digital volume correlation incliding rotational degrees of freedom during minimization”, *Experimental Mechanics*, vol. 42 no. 3, p. 272-278, 2002.

Synnergren P., Goldrein H.T., Proud W.G., “Application of digital speckle photography to flash x-ray studies of internal deformation fields in impact experiments”, *Applied Optics*, vol. 38 no. 19, p. 4030-4036, 1999.

Tillard-Ngan D., Etude de la rupture dans les géomatériaux cohésifs. Application à la marne de Beaucaire, PhD thesis, Grenoble University, 1992.

Verhulp E., van Rietbergen B., Huiskes R., “A three-dimensional digital image correlation technique for strain measurements in microstructures”, *Journal of Biomechanics*, vol. 37, p. 1313-1320, 2004.

Viggiani G., Lenoir N., Bésuelle P., Di Michiel M., Marello S., Desrues J., Kretzschmer M., “X-ray microtomography for studying localized deformation in fine-grained geomaterials under triaxial compression”, *C. R. Mécanique*, vol. 332, p. 819-826, 2004.

Vinegard H.J., de Waal J.A., Wellington S.L., “CT studies of brittle failure in Castlegate sandstone”, *International Journal of Rock Mechanics and Mining Sciences*, vol. 28, 1991, p. 441-448.

Zhang C., Rothfuchs T., “Experimental study of the hydro-mechanical behaviour of the Callovo-Oxfordian argillite”, *Applied Clay Science*, vol. 26, no. 1-4, p. 325-336, 2004.